Noise Characterization and Performance of MODIS Thermal Emissive Bands

Journal:	*Transactions on Geoscience and Remote Sensing*
Manuscript ID:	Draft
Manuscript Type:	Regular paper
Date Submitted by the Author:	n/a
Complete List of Authors:	Madhavan, Sriharsha; Science Systems and Applications, Inc, MCST/SSAI Xiong, Xiaoxiong; NASA, GSFC Wu, Aisheng; Science Systems and Applications Inc., HBSSS Wenny, Brian; Science Systems and Applications Inc., HBSSS Chiang, Kwofu; Science Systems and Applications, Inc., NASA/GSFC Chen, Na; Science Systems and Applications Inc., HBSSS Wang, Zhipeng; Science Systems and Applications Inc., HBSSS Li, Yonghong; Science Systems and Applications Inc., HBSSS
Keywords:	Remote sensing, Thermal variables measurement, Detectors

Noise Characterization and Performance of MODIS Thermal Emissive Bands

Sriharsha Madhavan[1], Xiaoxiong Xiong[2], Aisheng Wu[1], Brian Wenny[1], Kwofu Chiang[1], Na Chen[1], Zhipeng Wang[1], and Yonghong Li[1]

[1]Science and Systems Applications Inc, 10210, Greenbelt Road, Lanham, MD 20706
[2]Sciences and Exploration Directorate, NASA/GSFC, Greenbelt, MD 20771

Abstract

The MODerate-resolution Imaging Spectroradiometer (MODIS) is a premier Earth observing sensor of the early 21st Century, flying on-board the Terra (T) and Aqua (A) spacecrafts. Both instruments far exceeded their 6 year design life and continue to operate satisfactorily for more than 15 and 13 years, respectively. The MODIS instrument is designed to make observations at nearly a 100% duty cycle covering the entire Earth in less than 2 days. The MODIS sensor characteristics include a spectral coverage from 0.41 μm – 14.4 μm, of which those wavelengths ranging from 3.7 μm – 14. 4 μm cover the thermal infrared region which is interspaced in 16 Thermal Emissive Bands (TEB). Each of the TEB contains 10 detectors which record samples at a spatial resolution of 1 km. In order to ensure a high level of accuracy for the TEB measured Top Of Atmosphere (TOA) radiances, an onboard BlackBody (BB) is used as the calibration source. This paper reports the noise characterization and performance of the TEB on various counts. First, the stability of the onboard BB is evaluated to understand the effectiveness of the calibration source. Next, key noise metrics such as the Noise Equivalent Temperature difference (NEdT) and the Noise Equivalent dn difference (NEdN) for the various TEB are determined from multiple temperature sources. These sources include the nominally controlled BB temperature of 290 K for T-MODIS and 285 K for A-MODIS, as well as a BB Warm Up – Cool Down (WUCD) cycle that is performed over a temperature range from roughly 270 K – 315 K. The Space View (SV) port that measures the background signal serves as a viable cold temperature source for measuring noise. In addition, a well characterized Earth View (EV) Target, the Dome C site located in the Antarctic plateau, is used for characterizing the stability of the sensor, indirectly providing a measure of the NEdN. Based on this rigorous characterization, a list of the noisy and inoperable detectors for the TEB for both instruments is reported to provide the science user communities quality control of the MODIS Level 1B calibrated product.

Keywords: MODIS, Terra, Aqua, noise, NEdT, NEdN, calibration, blackbody, TEB

1. Introduction

Terra (T) and Aqua (A) are prime platforms for NASA's Earth Observing System (EOS) since launch in 1999 and 2002 respectively [1-4]. The T- platform is in a morning orbit with an equatorial crossing time of 10:30 am and the A- platform is in an afternoon orbit with an equatorial crossing time of 1:30 pm. Both platforms house a MODIS instrument that collectively allows the science community to better understand the Earth's energy budget on a daily basis. The MODIS instrument is a whiskbroom scanning radiometer, which has a 360° rotating double sided scan mirror and several On Board Calibrators (OBCs) as shown in Figure 1. The MODIS remotely collects information in 36 spectral bands varying from 0.41 μm to 14.4 μm, at three different spatial resolutions of 250 m, 500 m, and 1 km. The spectral wavelengths from 3.7 μm onwards cover the thermal infrared region which is separated into 16 Thermal Emissive Bands (TEBs).The 36 spectral bands are located on four Focal Plane Assemblies (FPAs) that comprises the visible (VIS), near infrared (NIR), short and middle wave infrared (SMIR) and the long wave infrared (LWIR) spectrum. The SMIR and LWIR FPAs house the thermal sensors which are maintained at a nominally cooled temperature of 83 K. Figure 2 shows the various FPAs along with the detector layout for each of the MODIS bands, the red square highlighting the cold FPAs, including all the TEB detectors. The superior nature of the MODIS instrument in comparison to the other heritage sensors such as AVHRR and Landsat TM is mainly due to

the sophisticated OBCs whose measurements are traceable to well characterized ground references. The OBCs include a Solar Diffuser (SD), a SD Stability Monitor (SDSM), a BlackBody (BB), a SpectroRadiometric Calibration Assembly (SRCA), and finally a Space View (SV) port. The SD and SDSM serve as a calibration source for the reflective solar bands [5]. The SRCA is used primarily to characterize the sensor's spatial and spectral stability [6-7]. The BB is designed for TEB calibration. And the SV is used to determine the background signal that would help remove the electronic offsets and thermal background from the actual measurements [8]. Figure 1 provides the setup of the various OBCs, in particular the BB is highlighted which is used for the detector calibration for each of the TEBs [9]. Table 1 gives the key design parameters, including the calibration requirements for the detector noise, and the primary application for each of the TEBs. The major instrument related events / operational changes for both T- and A- MODIS are noted in Tables 2 and 3 respectively. These events play a significant role in understanding the on orbit changes of the instrument telemetry, gains, and noise characteristics for all the bands. Several of these events happened in early life and since 2006 and 2005 no major changes in operation are reported for T- and A- MODIS.

The on-board calibration for TEBs of both MODIS instruments is based on accurate calibration radiances provided by the BB. The BB temperatures are accurately measured through a set of 12 thermistors that are uniformly embedded on the BB substrate [9]. These thermistors were extensively characterized pre launch, and are required to be within a temperature variability of ± 0.05 K. The layout of the various thermistors is shown in Figure 1. For T-MODIS the BB temperature is nominally controlled at 290K whereas A-MODIS is maintained at 285 K. Figures 3a. and 3b. shows the lifetime trends of the BB temperatures for both T- and A- MODIS at their set temperatures. The data presented is a weekly average of the 12 thermistors. Based on the lifetime trends, the variability of the BB temperatures is assessed to be within 15 mK for T-MODIS and within 5 mK for A-MODIS. As TEB detectors view the BB every scan, an almost instantaneous calibration is achieved, including the detector noise characteristics and gains. The TEB calibration equation is based on a quadratic model wherein the non linear terms become important when the TEB signal levels are at well below 0.3 $L_{typical}$ or close to 0.9 L_{max}. In order to characterize these terms, a periodic BB Warm-Up Cool-Down (WUCD) operation is executed. During this process the BB is varied from the instrument ambient temperature of close to 270 K to about 315 K, providing a valuable range to evaluate the non linear coefficients. Examples of a typical BB WUCD operation for both instruments are shown in Figures 5a and 5b.

In this paper, several aspects of the T- and A-MODIS TEBs noise characterization are examined. Following is the layout of the various sections. Section 2 provides the description of the TEB on orbit calibration equation and the definitions of the various noise parameters. These include the detector Signal-to-Noise Ratio (SNR), Noise Equivalent Temperature difference (NEdT), and Noise Equivalent dn difference (NEdN). These terms are measures of noise in the TEBs and serve as a key input to calibration uncertainty assessment [10]. Section 3 covers the methodologies used in the characterization of noise in the TEB detectors from various sources. These include the onboard BB, the SV, and reliable Earth View (EV) targets such as Dome Concordia (C). Section 4 provides the noise performance based on the methodologies described in section 3. Finally, section 5 gives the overall assessment of the noise levels of the detectors in TEBs and provides updated list of noisy and inoperable detectors that are used in the Quality Assurance (QA) Look Up Table (LUT) for the Level 1 B (L1B) processing.

2. On-Orbit Calibration and Noise Retrieval

The TEB calibration is based on a quadratic algorithm that converts the digital response of the detector to its at sensor aperture radiance. In order to perform the conversion, the digital response is first corrected for background and optical crosstalk (crosstalk correction only applied to T-MODIS Photo Conductive (PC) bands 32-36), which is represented in digital counts known as dn (digital number which is background subtracted response). The second step is to compute the calibration linear coefficient b_1 using the calibrator radiance (L_{CAL}) as observed from the nominally controlled BB temperature. Equations (1) and (2) summarize the calibration operation performed on all TEB channels on a scan by scan basis. The calibration terms a_0 and a_2 shown in equation (2) are evaluated on a

quarterly basis during the BB WUCD process. Details on the various calibration parameters shown in equation (1) and (2) can be found in various references [8-9, 11].

$$L_{CAL} = RVS_{BB}\varepsilon_{BB}L_{BB} + (RVS_{SV} - RVS_{BB})L_{SM} + RVS_{BB}(1-\varepsilon_{BB})\varepsilon_{cav}L_{cav} \quad (1)$$

$$b_1 = (L_{CAL} - a_0 - a_2 dn_{BB}^2)/dn_{BB} \quad (2)$$

In order to determine the noise metric NEdT, other key parameters needs to be defined. First, the frame-to-frame variations of the dn's (for example 50 frames of the BB or SV) at a fixed scan is computed, and is referred to as the NEdN or intrinsic noise of the detector. Further, an average estimate of the frame-by-frame deviations over the entire scans within a granule (scene) gives the average NEdN measured during roughly a 5 minute observation. Equation 3 gives the expansion of the above defined term:

$$NEdN = \sqrt{\frac{1}{N}\sum_{i=1}^{N}\left(DN_i - \overline{DN}\right)^2} \quad (3)$$

Where N is the total number of sampled scans and $\overline{DN}$ is the mean of DN_i (i = 1, 2, …N) (corresponds to Raw Digital Number i.e. no background subtraction). Next, the detector based SNR is defined when the sensor is looking at a constant source target (such as BB, instrument cavity, stable EV targets etc.) [12]. This is given as:

$$SNR = \overline{DN}/NEdN \quad (4)$$

As a first order approximation, the Noise Equivalent radiance difference (NEdL) at a corresponding radiance, say L_{CAL} as shown in equation 1, can be expressed as:

$$NEdL = L/SNR \quad (5)$$

Finally, combining all the terms defined in equations (3)-(5), the NEdT can be calculated as:

$$NEdT = \frac{NEdL}{dL/dT} \quad (6)$$

Where dL/dT is a function of spectral wavelength and temperature determined by Planck's equation. The above defined terms and the computation will be used in the same vigor while computing the noise estimates from various sources such as the nominally operated BB, BB WUCD events, SV, and EV targets.

3. Noise Characterization

This section is subdivided into 4 parts that describes the methodology to compute the noise metrics such as the NEdN and NEdT from various targets. First, the methodology to analyze the stability of the calibration sources is described, followed by noise measurements during nominal BB operation, during BB WUCD process, and finally noise estimation from stable EV targets such as Dome C.

3.1 BB stability and Background noise

The TEB calibration is based on a two point calibration comprised of the BB and SV signals. As mentioned earlier, the BB as a calibration source has been designed to meet a variability specification of 50 mK amongst the various BB thermistors. Though it is not critical, the long term weekly averaged BB temperatures of both instruments are also very stable and within design requirements. Since the TEB calibration is performed on a scan-by-scan basis, the

stability of the BB is necessary on shorter time scales. Hence, analyzing the deviation (stability) of the BB and noise levels of the background signal is quite essential in understanding the overall fidelity of the TEBs. With this objective in mind, two kinds of measurements are done. First, the short-term stability using 2 orbits of nominal BB data (roughly 200 minutes) is examined; the variations of its scan-by-scan temperatures and the corresponding standard deviations from all thermistors are computed. In order to understand the BB stability at various temperatures, the mean standard deviation of the BB temperature for each granule during WUCD event is also calculated and trended to see if the specification requirements are met. Second, the average NEdN measurements for the SV signal during nominal instrument operation for all the TEB is computed and trended temporally.

3.2 Noise at nominal BB operation

The evaluation of noise at nominal BB operation is essential for monitoring the performance of the detectors on a daily basis. As mentioned, the BB for T-MODIS is maintained at a nominal temperature of 290 K and A-MODIS at 285 K. Thus the NEdT can be computed for each scan at both BB temperature and $T_{typical}$ for the respective bands (refer Table 1). This is achieved by evaluating the partial derivative of the Planck's function as shown in Equation 6 at the above mentioned temperatures. Only data at nominal operating periods (no major instrument activity or anomaly) are chosen for the analysis. Further, the trends reported in this paper are on a weekly scale; however the noise trending for each TEB detector is performed on every available granule in the T- and A- MODIS OBC archive.

3.3 Noise during BB WUCD operation

The BB WUCD operation was primarily designed to track potential on-orbit changes in TEB detector nonlinear response. Since on-board BB temperature is limited to a smaller range from instrument ambient (approx. 270 K) to 315 K than pre-launch (P.L.) measurements from 170 K to 340 K, the accuracy of the nonlinear calibration coefficients determined from on-orbit BB WUCD may not be as good as that determined from P.L., especially at the low temperature end. The OBC BB WUCD operation also enables the TEB detector noise characterization to be made at different temperatures. The noise metrics NEdT, NEdN for the BB responses for the TEBs was trended and modeled as a function of BB temperature. Also, the NEdN for the SV response during the WUCD activity was trended and linearly modeled as a function of BB temperature as well. Since the CD activity is a slow passive process with no sudden changes of the BB temperatures as is the case with WU cycle, the noise trending would be relatively stable with a smooth relationship established for the NEdT vs BB temperature trend. For this purpose, the CD cycle is chosen for the noise analysis.

3.4 Noise estimation from EV target

Many EV sites serve as good references for sensor calibration and validation [13], [14]. One such EV site is Dome C. The Dome C site is one of the several summits of the Antarctica ice sheet and considered as the most homogeneous Earth target by the Concordia research stations jointly operated by France and Italy. With this site being well understood both vicariously and through cross sensor comparisons [15], allows a unique vantage point in assessing long-term instrument related drifts and changes. The scene temperature levels are below the 0.3 $T_{typical}$ for MODIS TEBs and hence an ideal test location for assessing the noise. Since certain amount of the signal is close to the background level, with exceptions to the land sensing channel such as MODIS band 31, it is somewhat possible to tease out the noise information within the signal. In order to give an idea of the actual geo location and the temperature levels at this site, Figure 12 gives an example of a 400 pixel × 400 pixel MODIS Band 31 image overlaid on the orthographic map projection of the Antarctic location that comprises the Dome C site. Also, the site being at the south pole of the Earth, most polar-orbiting remote sensing satellites such as MODIS have a unique advantage of making several overpasses in any given day. MODIS being a wide angle viewing spectroradiometer, the data in any given scan has response versus scan angle (RVS) dependencies [16]. Thus, in order to negate these impacts in the current study, only those scenes with nadir viewing angles are considered. For each scene, the standard deviation for each detector and each mirror side was computed separately over a small region of 20 × 20 MODIS area with the center pixel corresponding to the center latitude and longitude of Dome C. The standard

deviation is computed on scene pixels that cover a temperature range varying from approximately 200 K to approximately 210 K as measured by band 31. Finally, the standard deviation for each of the representative bands is modeled temporally over time. The modeled standard deviation from Dome C allows a stability check and is an indirect measure of the noise in EV pixels.

4. Noise Performance

This section provides a thorough analysis of the noise performance for both MODIS instruments based on the characterization approaches discussed above. Emphasis is placed on select TEBs and will be used as representative bands for detailed discussion. Also, for the TEBs the mirror side response differences are negligible and hence only mirror side 1 will be used as the representative [11].

First, the short-term stability for the on-board BB is presented. Figure 4a. shows the T-MODIS BB temperatures over two orbits of data during day 2012168 when the BB is normally controlled at 290 K. The temperatures during the daytime (and night time) portion of the orbits are plotted in red (blue). Similarly, the standard deviations of the BB temperatures in Figure 4a. are presented in Figure 4c. In general, the BB temperature scan-by-scan variations are within ±0.025 K. Typical standard deviations are approximately 0.03 K. Occasional telemetry noise was observed in both nighttime and daytime temperature telemetry for T-MODIS. Figures 4b. and 4d. illustrates the BB temperature short-term stability for A-MODIS during its nominal operation when the BB temperature is set at 285 K. Clearly, A-MODIS BB temperature is much more stable than T-MODIS. Its scan-by-scan variations are within ±0.005 K with essentially no daytime and nighttime difference. Typical BB temperature standard deviations are slightly less than 0.02 K. Compared to T-MODIS performance in Figure 4b., the BB temperature random noises in Figure 4d. are very small for A-MODIS.

As mentioned earlier, Figure 5a. shows a typical BB WUCD temperature profile for T-MODIS (averaged temperatures over 12 thermistors). It includes a portion of nominally controlled temperature profiles before and after the BB WUCD, when the BB is set at 290 K. During the WUCD process, the BB is set and operated at a number of intermediate temperatures between its ambient temperature and 315 K. It should be pointed out that the number of intermediate steps currently used is different from that used at the mission beginning. A similar BB WUCD profile for A-MODIS is illustrated in Figure 5b. The corresponding standard deviations for the two WUCD profiles are illustrated in Figures 5c. and 5d., where the horizontal lines shown are the requirements for the BB temperature stability. The entire BB WUCD operation takes more than 2 days to complete. Only the scan-averaged temperatures and standard deviations are shown. As expected, the results before and after the BB WUCD period in Figure 4 are consistent with those illustrated in Figure 5. It is clear from Figures 4-5 (d) that the A-MODIS BB has better short-term stability than T-MODIS at all temperatures.

Combining both the long-term and short-term trends, A-MODIS BB has performed exceedingly well; both instruments are meeting the design requirements satisfactorily for well over a decade.

The background noise is measured from the SV port and is given by the average NEdN metric as defined in section 2. Bands 20, 23, 27, 29, and 31-32 are chosen as representative bands for this analysis. Of which, bands 20 and 23 represent the Photo Voltaic (PV) MWIR channels, bands 27 and 29 represent the PV LWIR channels, and bands 31-32 are used to demonstrate performance of PC LWIR bands. Also, three representative detectors 1, 5, and 10 are chosen to portray the noise performance of the detector arrays in each of the TEB FPAs. Figure 6a.-f. shows the long-term NEdN trend measured from the SV response for the various TEBs of T-MODIS. These estimates characterize the intrinsic noise for each of the detectors. The NEdN on average, for all the three representative detectors, are stable and close to 1.0 and 1.1 for bands 20 and 23 (Figures 6a.and 6b.) respectively. In the case of PV LWIR bands 27 and 29 the NEdN trends (Figures 6c. and 6d.) for the three detectors have interesting characteristics. In the case of band 27 detector 1, the NEdN trends close to 1.3 until about 1200 days since epoch 2000. A sudden

jump is noticed around 1200 days when the NEdN is about 3.6. This is followed by a slow downward trend till 5500 days, to a value of approximately 2.6. Through extensive study by the MODIS Characterization Support Team (MCST), it is reported that from the year 2004 onwards, band 27 responses was significantly contaminated by electronic crosstalk [17-20]. The above mentioned NEdN behavior keeps in close trend with the severity of the electronic crosstalk effect. In fact, detector 1 was the worst affected by crosstalk [18-19]. In the case of detectors 5 and 10 the NEdN is stable till about 3500 days since epoch 2000. The increase in NEdN value to about 2.6 is also in trend with the increase in magnitude of crosstalk contamination for these detectors. Detector 5 is, however, stable much beyond 4000 days while detector 10 has tended to remain noisier. Recently, the work reported in [21] shows that all the PV LWIR bands (27-30) suffer from electronic crosstalk. However, bands 28-30 are less contaminated in comparison to band 27. Again, this is confirmed from the NEdN trends for band 29 (Figure 6d.). The three shown detectors are quite stable with NEdN estimate of approximately 0.85 till about 3500 days. From days 3500 onwards, a rise in NEdN is observed, to a value of approximately 1.9. Around 4200 days the NEdN is slightly reduced to about 1.0. More work is underway to characterize the impact of increase in noise for the PV LWIR bands. In contrast, the detectors of bands 31 and 32 are very stable with NEdN estimates hovering around 0.51 and 0.73 respectively. As a resemblance, the SV NEdN trends for T-MODIS representative bands show occasional jumps similar to the random telemetry noise seen in the T-MODIS BB stability trends.

Similar noise trends (as shown in Figure 6a.-f.) are presented in Figure 7a.-f. for A-MODIS. In comparison to T-MODIS the NEdN trends for A-MODIS are very stable. The NEdN for band 20 (Figure 7a.) are around 0.87 for detectors 1 and 5 whereas detector has a bias shift in the NEdN to approximately 1.14. Band 23 (Figure 7b.) is very stable as well with an average NEdN estimate between the three shown detectors is about 0.94. The PV LWIR bands 27 and 29 have a slightly higher fluctuation in the noise level probably caused by the electronic setting in these bands. The average NEdN estimates for band 27 (Figure 7c.) varies around 1.75 with a fluctuation of about 0.25 temporally. The PC bands 31-32 are very stable with average NEdN estimates of around 0.58 and 0.85 respectively. It is noted that A-MODIS bands 31 and 32 operate at a higher gain setting; thereby contributing to an increased bias in the noise levels when compared to T- MODIS.

The noise performance for each TEB detector is evaluated by the NEdT measurements at nominal BB operation, with the partial derivative component of the NEdT computed for typical scene temperatures. Tables 4 and 6 summarize the on-orbit noise performance for all the TEBs. The estimates shown are band averaged with the exclusion of noisy detectors. Also, the NEdT are yearly averaged and are shown for every two years since launch. From Table 4 some key aspects are highlighted. T-MODIS band 36 has a noisier performance throughout its lifetime and is about 0.44. This indeed was expected as P.L. testing had shown similar performance. The PV LWIR bands (27-30) of T-MODIS have tended to show a noisy response with 2014 averaged estimates being roughly 0.15, 0.06, 0.03, and 0.25 respectively. This, as mentioned earlier, is caused partly due to the aging sensor and partly due to the increased crosstalk contamination since 2010. In contrast, A-MODIS has a more stable noisy performance since launch (as seen in Table 6), with all the TEBs having their NEdT estimates to be well within the specification (provided in the second column). In order to highlight the key differences in the noise performance for T- and A-MODIS, the lifetime NEdT (weekly sampled, scan averaged) trends are provided. Figure 8 gives the NEdT trend for T-MODIS and is provided in two ways. The first subplot (Figure 8a.) shows the NEdT (normalized to the specification) trend for a representative noisy detector for bands 27-30. The representative detectors shown are band 27 detector 1, band 28 detector 8, band 29 detector 6, and band 30 detector 5. In each of the cases, it is clearly seen that the normalized NEdT changes with time and well within two to three times of the normalized requirement of 1.0. Further, the same data is used and the band averaged (including current good detectors (see Table 5) only) normalized NEdT is shown in Figure 8b. The trend clearly shows that these detectors meet the design specifications for the entirety of their performance. However, as mentioned earlier the noisy nature for these PV LWIR bands have increased since 2010. For comparison sakes, the normalized band averaged NEdT trends for A-MODIS PV LWIR bands are shown in Figure 9. Clearly, the noise requirements for A-MODIS have been met; furthermore, the noise levels are lower by at least a magnitude of 2 in comparison to the specification.

In general, most TEBs are well behaved for T- and A- MODIS with a large noise margin in comparison to the design requirements. Based on the noise characterization and performance trends, a rule of thumb for classifying noisy and inoperable was polished and updated in the Collection 6 L1B processing. The established rule for TEB detectors is as follows: A detector is flagged as 'Noisy' in the QA LUT when a) the percentage of scans within a granule with NEdT exceeding specification is greater than 20% consistently for a period of two weeks, and b) scan-by-scan b_1 displays fluctuations from it's previous stable value. A detector is flagged as 'Inoperable' in the QA LUT when the granule average NEdT continuously exceeds 2 times specification for a period of two weeks. If the detectors return back to its pre-anomalous stage and exhibit stable behavior for a period of 2 weeks, the status of the detector could be re-classified to its pre-anomaly state. Based on the noise performance and its criteria, a list of TEB detectors that are classified to be noisy and inoperable for both T-and A- MODIS are summarized in Tables 5 and 7 respectively. For T- MODIS: At P.L. 30 detectors were characterized as 'noisy' in terms of performance. First light (nadir door open) showed 35 noisy detectors based on OBC measurements. Currently, 47 detectors (of which 24 are TEB detectors) have been classified to be noisy in operation with no inoperable detectors. Most of the recent TEB detectors (since last five years) classified to be noisy were related to the passage of the satellite over the South Atlantic Region and often termed as South Atlantic Anomaly (SAA) [22]. For A-MODIS, at P.L. 10 detectors (1 TEB detector) were found to be inoperable and 2 detectors (1 TEB detector) as noisy. After over 12 years in orbit A-MODIS has only 4 noisy TEB detectors out of 7 noisy detectors (RSBs and TEBs included) and 1 inoperable TEB detector out of 15 inoperable detectors (RSBs and TEBs included).

The noise performance is now analyzed as a function of varying temperatures. This is done in two ways. First, the noise results from BB CD will be presented, followed by the noise estimates from the Dome C EV target. Figure 10. gives two examples of NEdT (a.-b.), NEdN SV (c.-d.) as functions of BB temperatures: one in 2004 and the other in 2014. Also marked in Fig. 10 (a.-b.) are the specified typical temperatures and corresponding NEdT requirement. From the NEdT trends it is quite clear that all the representative bands (20, 23, 29, 31, and 32) meet the requirement from about 270 K and above, with exceptions for bands 20 and 23. It is noted that the increase in NEdT at lower temperatures is an artifact of the derivative term dT/dL. The change in small amount of L would cause dramatic increase in the derivative term according to the Planck function. This typically is the case for the MWIR bands (ex: bands 20 and 23). However, this does not translate into an actual increase in noise as NEdN is more or less stable for the temperature range of 270 K – 315 K. The NEdN estimates from the SV response during the CD period are quite stable and are very comparable to the long term NEdN estimates during nominal BB operation. Further no discernible change is observed in the NEdT trends for the two CD events. This indicates that the instrument performance has been quite stable over the years. Similar results are presented for A-MODIS in Figure 11. (a.-d.). The noise performance is very similar to the one observed for T-MODIS.

As mentioned earlier, in order to understand the noise performance at a much colder temperature range, the Dome C target was used and the standard deviation of the sensor digital response was performed as mentioned in section 3.4. Figure 13 shows the temporal characterization for the same bands as used in the CD analysis. A linear model was fitted for each of the bands. Based on the modeling, the standard deviations for bands 20, and 23 remain quite stable throughout the mission lifetime, which is expected. Since these bands sense very little signal, with the radiance levels being close to background, they show a stable behavior. However, in the case of land sensing channels, such as bands 29, 31 and 32, the responses contain a higher portion of signal, and any variability seen is a mixture of both signal and noise. This makes it difficult to distinguish the actual noise from the measured standard deviations. However, a stable standard deviation measurement temporally does give confidence that the NEdN would also behave in a similar fashion. The results for A-MODIS are shown in Figure 14. Similar observations are drawn for A-MODIS as well. Thus, both sources i.e. BB CD event and varying Dome C temperatures corroborate the noise performance very well.

Table 8 nicely summarizes the noise characterization from Dome C site. The characterized slopes for the representative bands and the two MODIS instruments are provided. Based on the results, the slopes (rate of change) for T-MODIS is very small with the largest change for band 29 which has a negative change of approximately -0.018. In comparison, A-MODIS has shown greater change in terms of slope for the standard deviation for bands 31 and 32. The slopes were approximately 0.11 and 0.13 respectively. This is very consistent to the NEdN results for SV response, and is attributed to the earlier noted high gain setting for these two bands. For bands 20, 23 and 29, A-MODIS has very similar trends to T-MODIS. Based on the provided results, T-MODIS has tended to show very consistent results from the three sources (i.e. BB, SV, and EV target).

5. Summary

MODIS is a key Earth remote sensing instrument that is onboard the T- and A- spacecraft. Both instruments continue to operate satisfactorily over their current lifetime of 15 years and 13 years respectively. In particular, the TEB performance has been quite astounding in comparison to its predecessors such as AVHRR and very comparable to the next generation sensors such as Suomi-NPP VIIRS [23]. The high fidelity of the TEB performance is attributed to the on-orbit scan-by-scan calibration that is based on the BB and SV sources. The results and approach presented in this paper will be very useful to sensors such as Suomi NPP VIIRS and beyond, as the analysis and discussion presented has likeness to the VIIRS bands. Furthermore, the NEdT measurement is a vital component for the Uncertainty Index reported in the MODIS L1B products.

The noise characterization metrics such as NEdN and NEdT measured from various sources helped establish the noise levels of the two MODIS instruments to a great deal of accuracy. The NEdT measurements at nominal BB operation temperatures evaluated the performance of the TEB detectors at typical radiance levels, and ensured the requirements are met as per the design specifications for most of the lifetime. A handful of detectors in the T-MODIS LWIR bands have found to be within two to three times of the NEdT specification. The NEdT measurements at varying BB temperatures allowed the analysis to see the noise deviation from the normal operating range. Over the lifetime of both instruments the NEdT and NEdN measurements from the BB source showed slightly larger estimates by about 1~2 % from the design specifications which are applicable only for typical radiance levels. The ground target study using Dome C, that generally correspond to signal levels of less than 0.3 $L_{typical}$ radiance levels, demonstrated that the sensor digital response standard deviations are indeed stable, and in-directly keeping in trend with the BB and SV sources.

The results of this study indicate that both T- and A- MODIS TEB detectors are maintained to be stable temporally and radiometrically over a wide sensor range. Thus, both MODIS instruments continue to provide very high quality remote sensing data of the Earth for well over a decade, their products significantly helping the society worldwide.

Acknowledgements

The authors would like to thank all current (in particular Jake Brinkmann for proof reading the article) and past members of the MCST for their many and varied contributions over the years. In addition thanks go to the science team members we have collaborated with, leading to greater understanding of instrument performance, impacts on the science products and improvements in our calibration methodologies.

References

[1] C.L. Parkinson, “Summarizing the first ten years of NASA’s Aqua mission,” IEEE Journal of Selected Topics in Applied Earth Observations and Remote Sensing,**6**(3), 1179-1188, 2013.

[2] C.O. Justice, E. Vermote, J.R.G. Townshend, R. Defries, D.P. Roy, D.K. Hall, V.V. Salomonson, J.L. Privette, G. Riggs, A. Strahler, W. Lucht, R.B. Myneni, P. Lewis, and M.J. Barnsley, "The Moderate Resolution Imaging Spectroradiometer (MODIS): Land Remote Sensing for Global Change Research," *IEEE Trans. Geosci. Remote Sensing*, **36**, 1228-1249 (1998) [doi:10.1109/36.701075].

[3] W.E. Esaias, M.R. Abbott, I. Barton, O.W. Brown, J.W. Campbell, K.L. Carder, D.K. Clark, R.L. Evans, F.E. Hoge, H.R. Gordon, W.P. Balch, R. Letelier, and P.J. Minnett, "An Overview of MODIS Capabilities for Ocean Science Observations," *IEEE Trans. Geosci. Remote Sensing*, **36**, 1250-1265 (1998) [doi:10.1109/36.701076].

[4] M.D. King, W.P. Menzel, Y.J. Kaufman, D. Tanre, B.C. Gao, S. Platnick, S.A. Ackerman, L.A. Remer, R. Pincus, and P.A. Hubanks, "Cloud and Aerosol Properties, Precipitable Water, and Profiles of Temperature and Water Vapor from MODIS," *IEEE Trans. Geosci. Remote Sensing*, **41**, 442-458 (2003) [doi:10.1109/TGRS.2002.808226].

[5] X. Xiong, J. Sun, W. Barnes, V. Salomonson, J. Esposito, H. Erives, and B. Guenther,"Multiyear on-orbit calibration and performance of Terra MODIS reflective solar bands," *IEEE Trans. Geosci. Remote Sensing*, vol. 45, no. 4, 879-889, 2007.

[6] X. Xiong, N. Che, and W. Barnes, "Terra MODIS on-orbit spatial characterization and performance", *IEEE Trans. Geosci. Remote Sensing*, vol. 43, no. 2, 355-365, 2005.

[7]X. Xiong, N. Che, and W. Barnes, "Terra MODIS on-orbit spectral characterization and performance", *IEEE Trans. Geosci. Remote Sensing*, vol. 44, no. 8, 2198-2206, 2006.

[8]Xiong, X., K. Chiang, J. Esposito, B. Guenther, and W. Barnes, "MODIS On-Orbit Calibration and Characterization", Metrologia, vol. 40, issue 1, pp. 89-92, 2003.

[9] Xiong, X., B. Wenny, A. Wu, and W. Barnes, "MODIS On-board Blackbody Function and Performance", IEEE Trans. Geosci. Remote Sens., vol. 47, issue 10, 2009.

[10] K. Chiang, X. Xiong, A. Wu, and W. Barnes, "MODIS thermal emissive bands calibration uncertainty analysis, Earth Observing Systems IX", *Proc. SPIE*, vol. 5542, pp. 437-447, 2004.

[11] X. Xiong, A. Wu, B. N. Wenny, S. Madhavan, Z. Wang, Y. Li, N. Chen, W. Barnes, and V. Salomonson, "Terra and Aqua MODIS Thermal Emissive Bands On-orbit Calibration and Performance", IEEE Trans. Geosci. Remote Sens., (accepted), 2015.

[12] A. Wu, and X. Xiong, "Determination of Noise Characterization of MODIS Thermal Emissive Bands for Cold Scene Observations, Earth Observing Systems XIII", *Proc. SPIE*, vol. 7081, no. 70810F, 2008.

[13] D. L. Helder, K. Thome, N. Mishra, G. Chander, X. Xiong, A. Angal, and T. Choi, "Absolute Radiometric Calibration of Landsat Using a Pseudo Invariant Calibration Site", *IEEE Transactions on Geoscience and Remote Sensing*, vol. 51, issue 3, pp. 1360-1369, 2013.

[14] T. Choi, X. Xiong, A. Angal, G. Chander, and J. Qu, "Assessment of the spectral stability of Libya 4, Libya 1, and Mauritania 2 sites using Earth Observing One Hyperion", *Journal of Applied Remote Sensing*, vol. 8, issue 1, 2014.

[15] B. N. Wenny and X. Xiong, "Using a cold earth surface target to characterize long-term stability of the MODIS thermal emissive bands," *IEEE Geosci. Remote Sens. Lett.*, vol. 5, no. 2, pp. 162–165, Apr. 2008.

[16] J. Sun, X. Xiong, A. Angal, H. Chen, A. Wu, and X. Geng, "Timedependent response versus scan angle for MODIS reflective solar bands," *IEEE Trans. Geosci. Remote Sens.*, vol. 52, No. 6, 3159-3174, 2014.

[17] J. Sun, S. Madhavan, B. Wenny, and X. Xiong, "Terra MODIS band 27 electronic crosstalk: cause, impact, and mitigation", Proceedings of SPIE – Sensors, Systems, and Next-Generation Satellites XV, vol. 8176, no. 81760Z, 2011.

[18] J. Sun, X. Xiong, S. Madhavan, and B. N. Wenny, "Terra MODIS Band 27 Electronic Crosstalk Effect and Its Removal", *IEEE Trans. Geosci. Remote Sens.* 52, 1551-1561, 2014.

[19] J. Sun, X. Xiong, Y. Li, S. Madhavan, A. Wu, and B. N. Wenny, "Evaluation of Radiometric Improvements With Electronic Crosstalk Correction for Terra MODIS Band 27", *IEEE Trans. Geosci. Remote Sens*. 52, 6497-6507, 2014.

[20] S. Madhavan, J. Sun, X. Xiong, B. N. Wenny, and A. Wu, "Statistical analysis of the electronic crosstalk correction in Terra MODIS Band 27 ", Proc. SPIE 9218, Earth Observing Systems XIX, 921824, 2014.

[21] J. Sun, S. Madhavan, X. Xiong, and M. Wang, "Electronic crosstalk correction for terra long wave infrared photovoltaic bands ", Proc. SPIE 9264, Earth Observing Missions and Sensors: Development, Implementation, and Characterization III, 926412, 2014.

[22] J. Dodd, B. Wenny, K. Chiang, and X. Xiong, "Space environment's effect of MODIS calibration", *Proceedings of SPIE – Post-launch Calibration and Validation I*, vol. 7807, no. 78070G, 2010.

[23] X. Xiong, J. Butler, A. Wu, V. Chiang, B. Efremova, S. Madhavan, J. Mcintire, and H. Oudrari, "Comparison of MODIS and VIIRS onboard blackbody performance", Proc. SPIE 8533, Sensors, Systems, and Next-Generation Satellites XVI, 853318, 2012.

List of Tables:

List of Figures:

Fig. 13. Standard deviation characterization of Dome C EV site for representative bands of T-MODIS

Fig. 14. Standard deviation characterization of Dome C EV site for representative bands of A-MODIS

Table 1. MODIS spectral band design specifications. CW is center wavelength in μm; BW is bandwidth in μm; Ttyp is typical temperature in K; NEdT is noise equivalent difference temperature in K.

TEB Band	CW	BW	Ttyp	NEdT	Primary Use
20	3.75	0.18	300	0.05	Surface/cloud temperature
21	3.96	0.06	335	0.20	
22	3.96	0.06	300	0.07	
23	4.05	0.06	300	0.07	
24	4.47	0.07	250	0.25	Atmospheric temperature
25	4.52	0.07	275	0.25	
27	6.72	0.36	240	0.25	Water vapor
28	7.33	0.30	250	0.25	
29	8.55	0.30	300	0.05	Cloud properties
30	9.73	0.30	250	0.25	Ozone
31	11.03	0.50	300	0.05	Surface/cloud temperature
32	12.02	0.50	300	0.05	
33	13.34	0.30	260	0.25	Cloud top altitude
34	13.64	0.30	250	0.25	
35	13.94	0.30	240	0.25	
36	14.24	0.30	220	0.35	

Table 2. Important spacecraft and instrument events for T-MODIS

Date	Event Description
12/18/99	Terra launch
02/13/00	Science Mode, A-side electronics
02/24/00	First light; nadir aperture door open
06/08/00	Cold focal plane assembly stopped controlling temperature
08/03/00	Focal plane assembly temperature set to 85K
08/05/00	Formatter reset anomaly; MODIS enters standby mode, then safe mode
10/30/00	MODIS switches to B-side electronics configuration
06/15/01	Power supply 2 (PS2) B-side shutdown (Safe Mode)
07/02/01	MODIS switches to A-side electronics configuration using PS1
03/19/02	Spacecraft safe mode hold anomaly during maneuver
09/17/02	Switch to B-side formatter; other components remain on A-side
05/06/03	Solar diffuser door fails to open when commanded
07/02/03	Solar diffuser door set to remain open with screen down
12/16/03	Attitude Control Electronics anomaly; S/C transition to safe mode
11/22/04	SRCA 10W lamp #2 fails to operate normally
02/18/06	SRCA 10W lamp #3 becomes abnormal and is taken out of service
08/22/06	Nadir aperture door and SV door inadvertently closed

Table 3. Important spacecraft and instrument events for A-MODIS

Date	Event Description
05/04/02	Aqua launch
06/07/02	Science Mode, B-side electronics
06/24/02	First light; nadir aperture door open
06/27/02	Spacecraft in safe mode due to a single event upset (SEU)
07/29/02	Spacecraft in safe hold due to spacecraft anomaly
08/09/02	SD door open as command was accidentally dropped; door closed 08/14/02
09/12/02	S/C in safe hold due to ephemeris error; recovered fine pointing same day
04/14/03	SRCA 10W lamp #2 is taken out of service
06/28/05	SRCA 10W lamp #3 is taken out of service

Table 4. T-MODIS Detector Noise (NEdT) Characterization Results at $L_{Typical}$

Band	SPEC.	P.L.	2000	2002	2004	2006	2008	2010	2012	2014
20	0.05	0.03	0.03	0.03	0.03	0.03	0.03	0.03	0.03	0.03
21	0.20	0.17	0.16	0.17	0.17	0.15	0.16	0.16	0.15	0.16
22	0.07	0.03	0.03	0.03	0.03	0.03	0.03	0.03	0.03	0.03
23	0.07	0.02	0.02	0.02	0.02	0.02	0.02	0.02	0.02	0.02
24	0.25	0.13	0.16	0.13	0.13	0.13	0.13	0.13	0.13	0.13
25	0.25	0.06	0.06	0.05	0.05	0.05	0.05	0.05	0.05	0.05
27	0.25	0.10	0.09	0.09	0.09	0.10	0.11	0.13	0.11	0.15
28	0.25	0.04	0.06	0.06	0.06	0.06	0.08	0.09	0.06	0.06
29	0.05	0.02	0.02	0.02	0.02	0.02	0.03	0.03	0.03	0.03
30	0.25	0.09	0.10	0.10	0.10	0.10	0.12	0.17	0.13	0.25
31	0.05	0.03	0.03	0.02	0.03	0.03	0.03	0.03	0.03	0.03
32	0.05	0.04	0.04	0.04	0.04	0.04	0.04	0.04	0.04	0.04
33	0.25	0.14	0.13	0.13	0.13	0.13	0.13	0.13	0.13	0.13
34	0.25	0.20	0.20	0.20	0.19	0.19	0.19	0.19	0.19	0.20
35	0.25	0.24	0.24	0.23	0.23	0.23	0.23	0.23	0.23	0.23
36	0.35	0.45	0.44	0.43	0.44	0.44	0.44	0.44	0.44	0.44

Table 5. T-MODIS noisy detectors

Time	Event	Noisy Band (Detector)
Pre-launch		B7(all), B36(all)
2000055.1527	Nadir Door Open	B5(4,16), B7(all), B33(1), B34(7,8), B36(all)
2000160.0000	CFPA Lost Control	B5(4,16), B7(all), B30(5) B33(1), B34(7,8), B36(all)
2000218.2210	Formatter Anomaly	B5(4,16), B7(all), B27(6), B30(5), B33(1), B34(6,7,8), B36(all)
2000304.1420	Switch to B-Side	B5(4,16), B7(all), B27(6), B30(5), B33(1), B34(6,7,8), B36(all)
2001019.1415	N/A	B5(4,16), B7(all), B27(6), B30(5, 8), B33(1), B34(6,7,8), B36(all)
2001183.2245	Switch to A-Side	B5(4), B7(all), B27(6), B30(5, 8), B33(1), B34(6,7,8), B36(all)
2002078.1615	Safe Mode	B5(4), B7(all), B27(6), B28(3), B30(5,8), B33(1), B34(5,6,7,8), B36(all)
2003350.1305	Safe Mode	B5(4), B7(all), B27(1,6), B28(8), B30(5,8), B33(1), B34(6,7,8), B36(all)
2005130.1345	SAA (Day)	B5(4), B7(all), B27(1,6), B28(1,8), B29(6), B30(5,8), B33(1), B34(6,7,8), B36(all)
2005309.1510	N/A	B5(4), B7(all), B27(1,6), B28(8,9), B29(6), B30(5,8), B33(1), B34(6,7,8), B36(all)
2006155.0210	SAA (Night)	B5(4), B7(all), B27(1,6), B28(8), B29(6), B30(3,5,8), B33(1), B34(6,7,8), B36(all)
2007193.1155	SAA (Day)	B5(4), B7(all), B27(1,6), B28(8), B29(6), B30(3,5,8), B33(1), B34(6,7,8), B36(all)
2008308.0900	SAA (Night)	B5(4), B7(all), B27(1,2,6), B28(8), B29(6), B30(1,3,5,8), B33(1), B34(6,7,8), B36(all)
2013125.1740	SAA (Night)	B5(4), B7(all), B27(1,2,6), B28(8), B29(6), B30(1,3,5,7,8), B33(1), B34(6,7,8), B36(all)

Table 6. A-MODIS Detector Noise (NEdT) Characterization Results at $L_{Typical}$

Band	SPEC.	P.L.	2002	2004	2006	2008	2010	2012	2014
20	0.05	0.02	0.02	0.02	0.02	0.02	0.02	0.02	0.02
21	0.20	0.23	0.21	0.19	0.20	0.21	0.21	0.19	0.19
22	0.07	0.02	0.02	0.02	0.02	0.02	0.02	0.02	0.02
23	0.07	0.02	0.02	0.02	0.02	0.02	0.02	0.02	0.02
24	0.25	0.13	0.11	0.11	0.11	0.11	0.11	0.11	0.11
25	0.25	0.04	0.04	0.04	0.04	0.04	0.04	0.04	0.04
27	0.25	0.09	0.10	0.10	0.10	0.09	0.10	0.10	0.10
28	0.25	0.05	0.05	0.05	0.05	0.05	0.05	0.05	0.05
29	0.05	0.02	0.02	0.02	0.02	0.02	0.02	0.02	0.02
30	0.25	0.09	0.08	0.08	0.09	0.08	0.09	0.09	0.09
31	0.05	0.02	0.02	0.02	0.02	0.02	0.02	0.02	0.02
32	0.05	0.03	0.03	0.03	0.03	0.03	0.03	0.03	0.03
33	0.25	0.08	0.08	0.08	0.08	0.08	0.08	0.08	0.08
34	0.25	0.12	0.12	0.12	0.12	0.12	0.12	0.12	0.12
35	0.25	0.13	0.15	0.15	0.15	0.15	0.15	0.15	0.15
36	0.35	0.25	0.23	0.23	0.23	0.23	0.23	0.23	0.23

Table 7. A-MODIS noisy and inoperable detectors

Time	Event	Noisy Band (Detector)	Inoperable Band (Detector)
Pre-launch		B6(17), B20(10)	B5(20), B6(2,12-14,16,18-20), B36(5)
2002175.2324	Nadir Door Open	B6(7,9,17)	B5(20), B6(2,4-6,10,12-16,18-20), B36(5)
2005010.1715	SAA (Day)	B6(7,9,17), B27(3)	B5(20), B6(2,4-6,10,12-16,18-20), B36(5)
2007359.1020	N/A	B6(7,9,17), B27(3), B29(8)	B5(20), B6(2,4-6,10,12-16,18-20), B36(5)
2008038.1750	SAA (Day)	B6(7,9,17), B27(3), B29(2,8)	B5(20), B6(2,4-6,10,12-16,18-20), B36(5)
2012022.1510	SAA (Day)	B6(7,9,17), B27(3), B29(2,6,8)	B5(20), B6(2,4-6,10,12-16,18-20), B36(5)

Table 8. Long-term standard deviation slope assessed using Dome C EV site

Band	T-MODIS Dome C Deviation (Slope)	A-MODIS Dome C Deviation (Slope)
20	-0.0016	-0.0010
23	0.0003	0.0007
29	-0.0182	0.0613
31	-0.0061	0.1123
32	-0.0096	0.1347

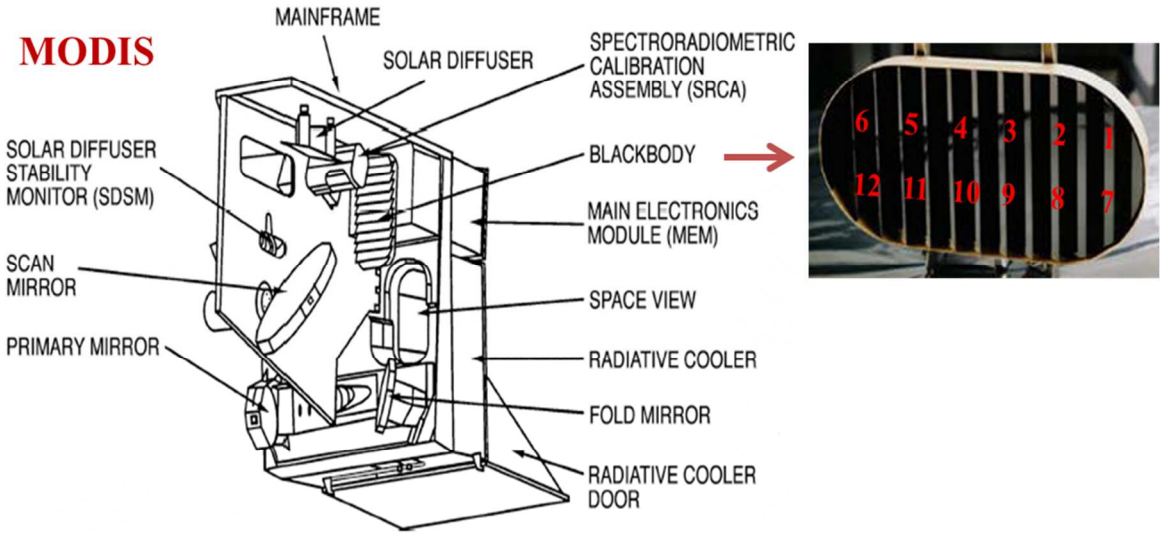

Fig. 1. MODIS Instrument setup with On-board Calibrators

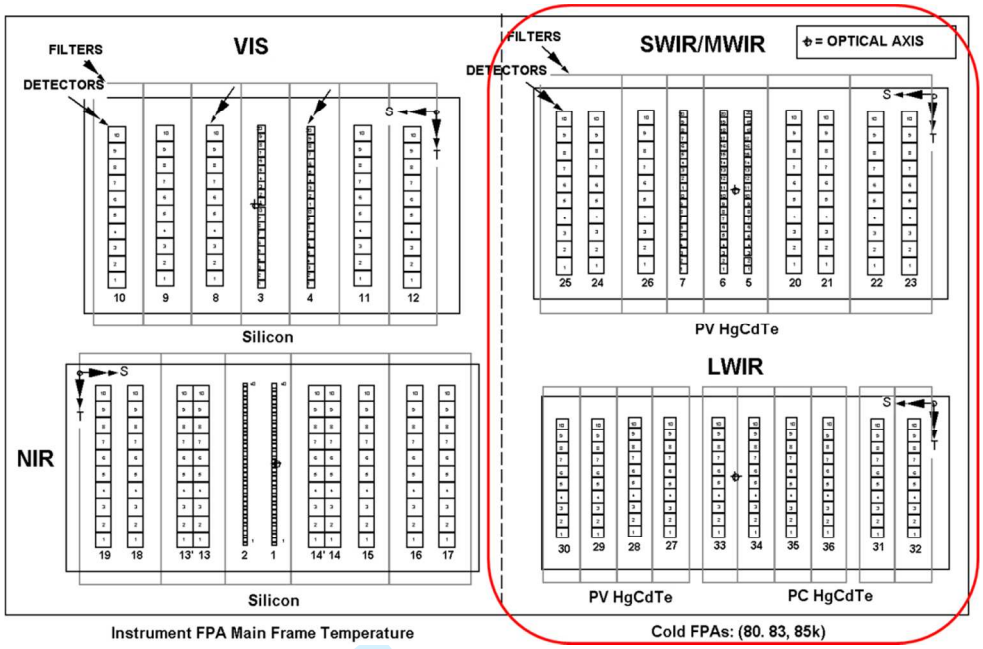

Fig. 2. MODIS Focal Plane layout (red box highlighting the TEB)

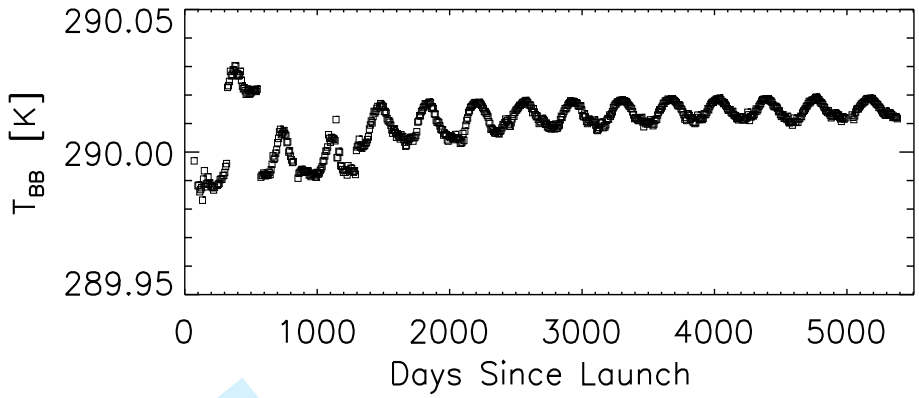

a.

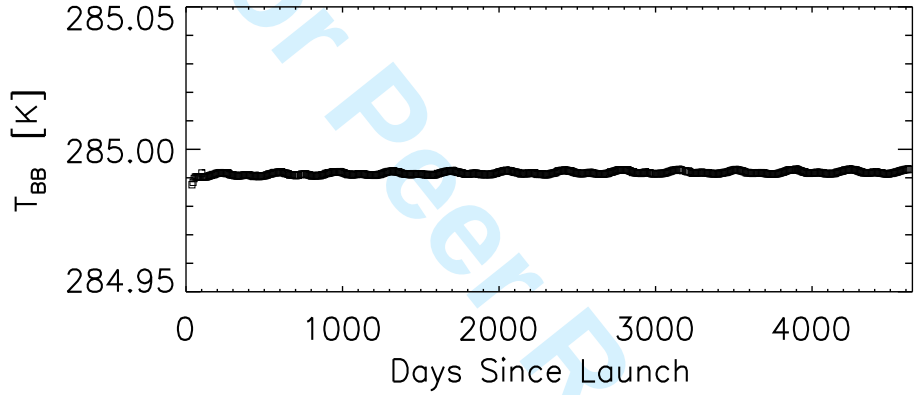

b.

Fig. 3. Long-term BB temperature (weekly averaged) a. T-MODIS, b. A-MODIS

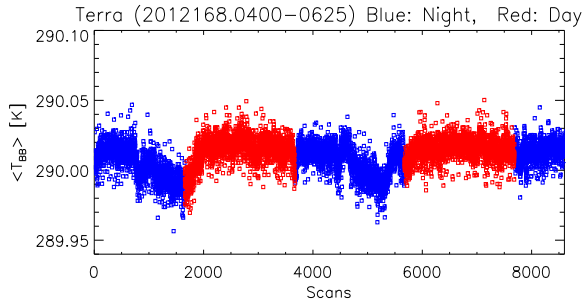

a.

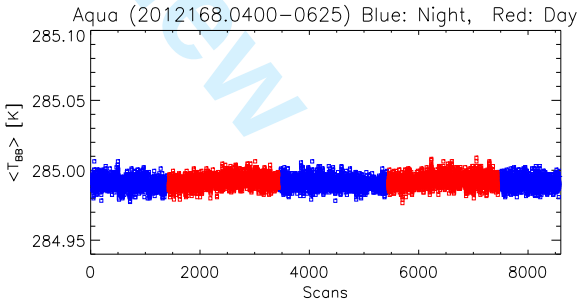

b.

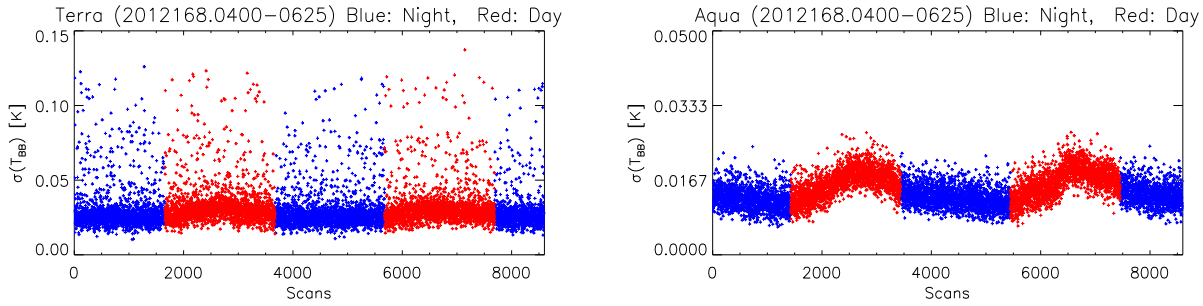

c. **d.**

Fig. 4. Illustration of short term scan-by-scan temperatures of BB and its corresponding standard deviations a., c. T-MODIS, b., d. A-MODIS

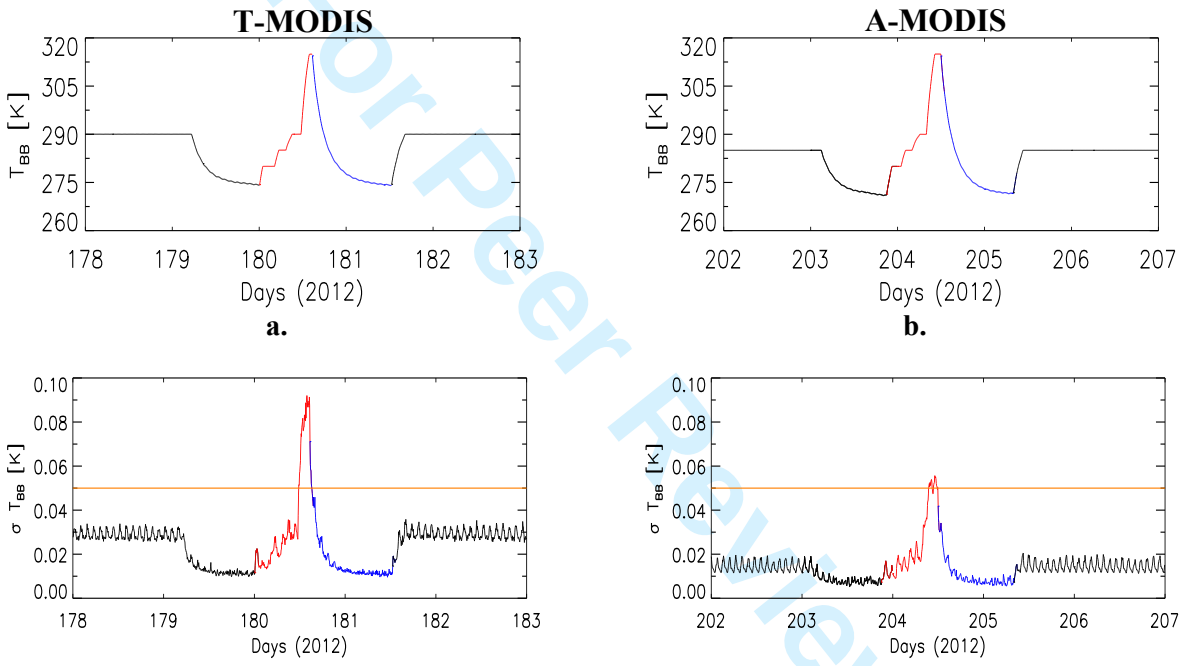

a. **b.**

c. **d.**

Fig. 5. Typical BB WUCD temperature profiles and the corresponding standard deviations during the event. a., c. T-MODIS, b., d. A-MODIS

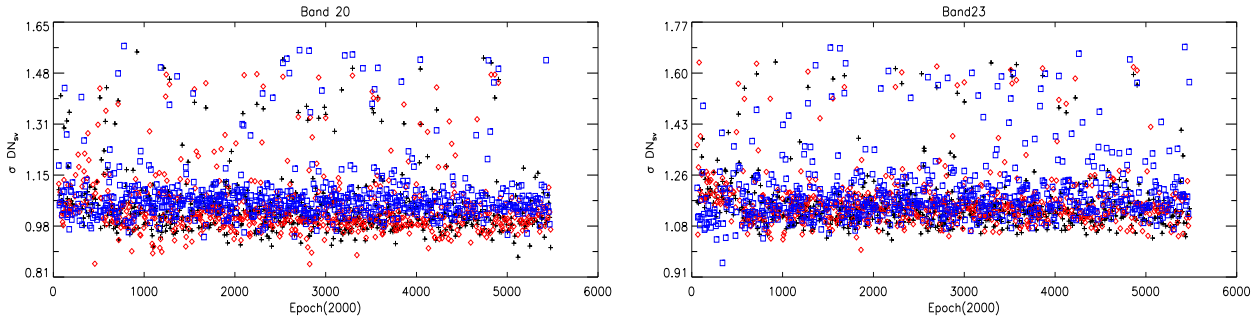

a. **b.**

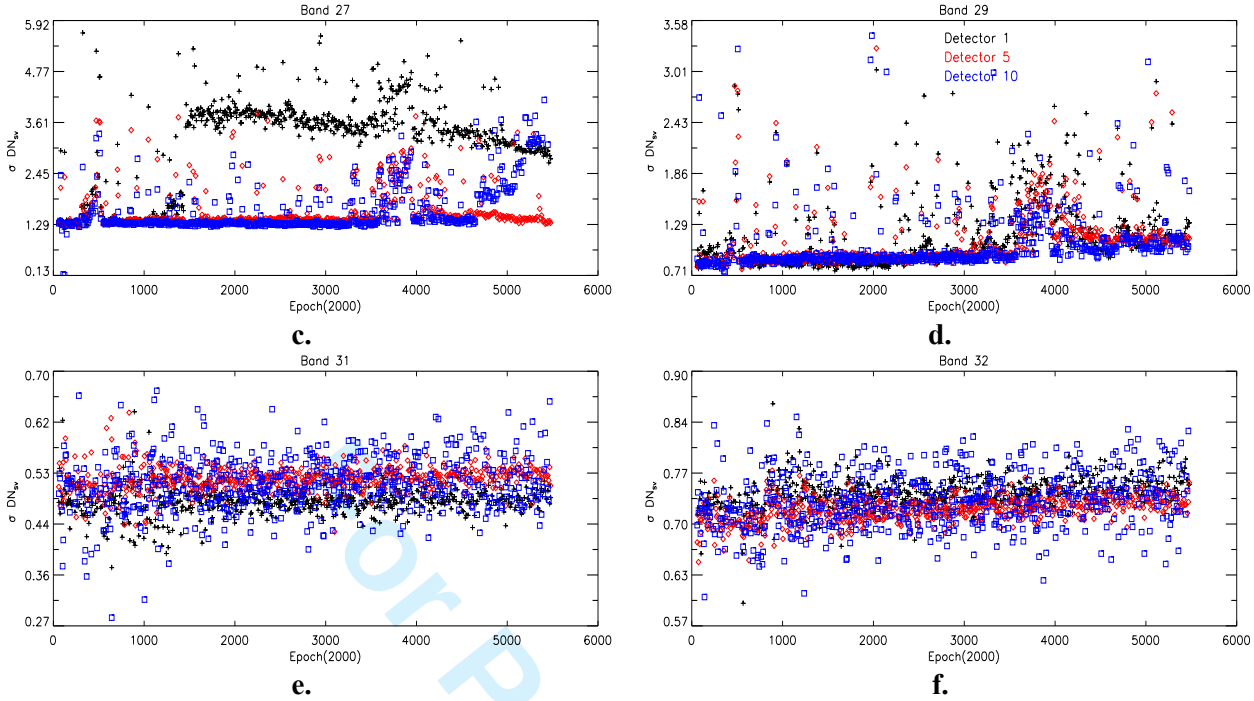

Fig. 6. Long-term NEdN trending of SV for representative bands of T-MODIS a. Band 20, b. Band 23, c. Band 27, d. Band 29, e. Band 31, f. Band 32

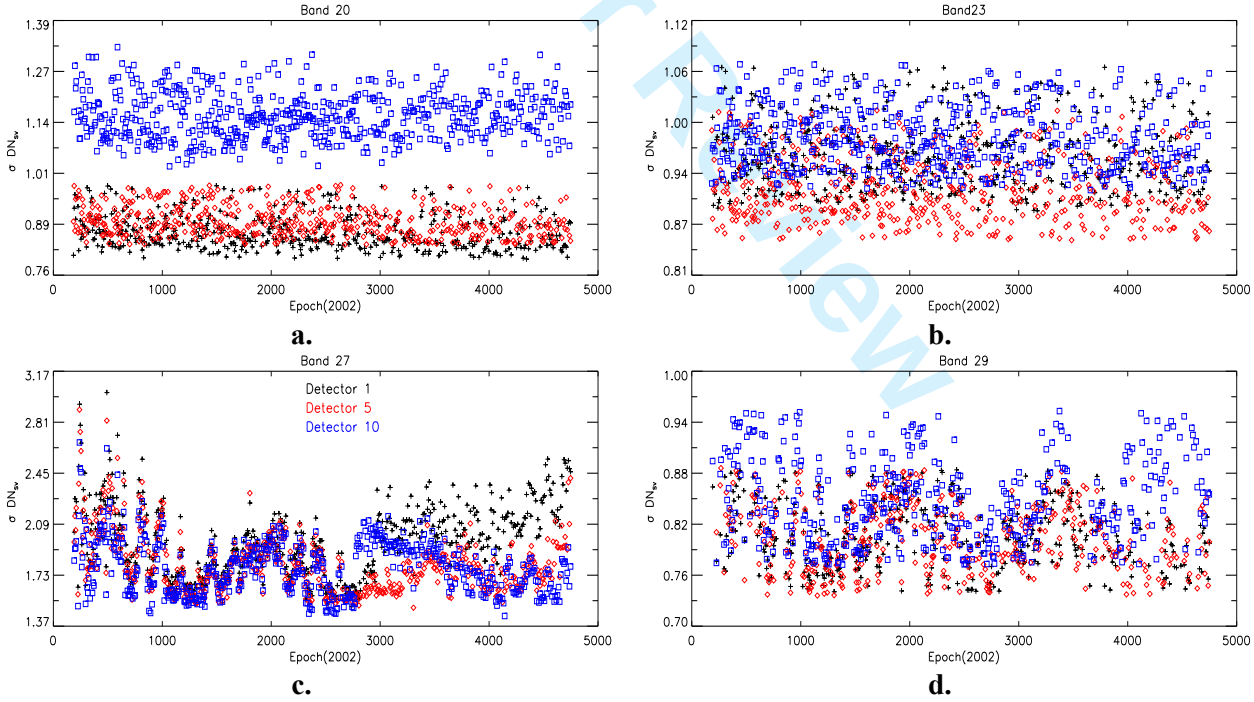

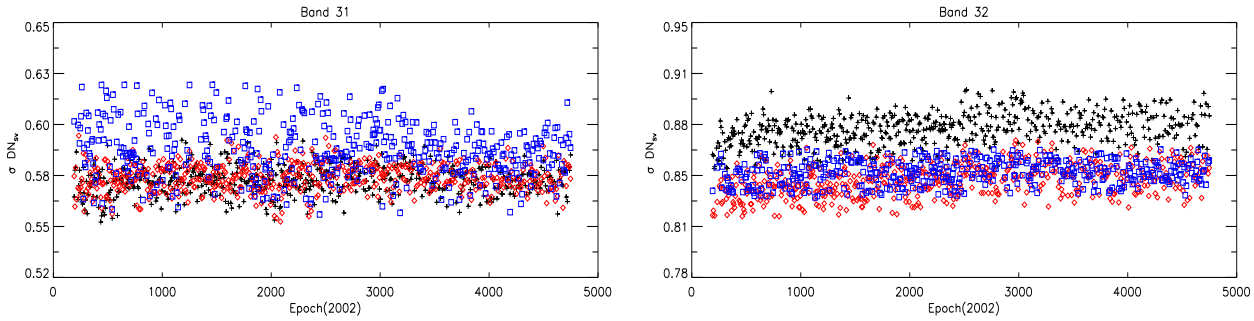

e. f.

Fig. 7. Long-term NEdN trending of SV for representative bands of A-MODIS a. Band 20, b. Band 23, c. Band 27, d. Band 29, e. Band 31, f. Band 32

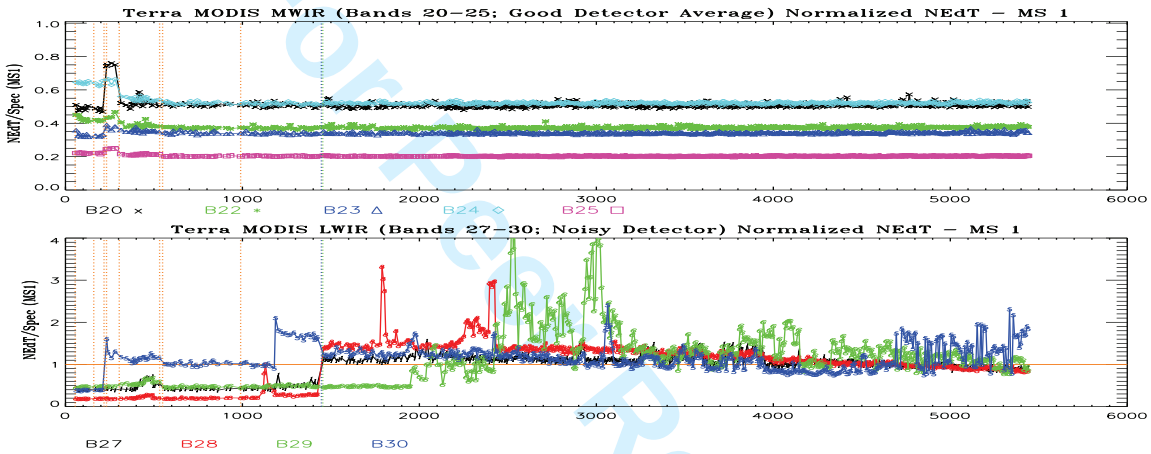

a.

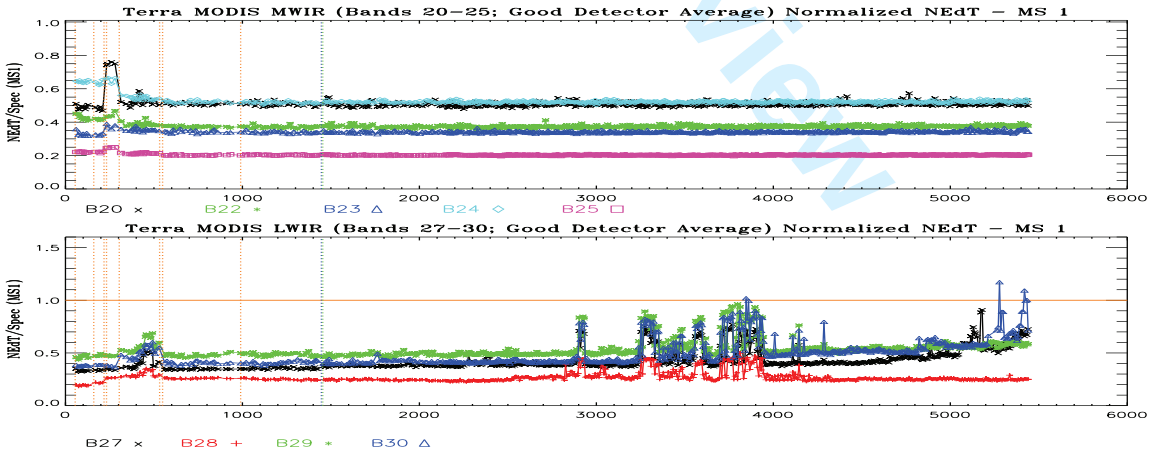

b.

Fig. 8. Long-term NEdT trending for PV LWIR bands of T-MODIS a. Representative Noisy detector, b. Good detector Average

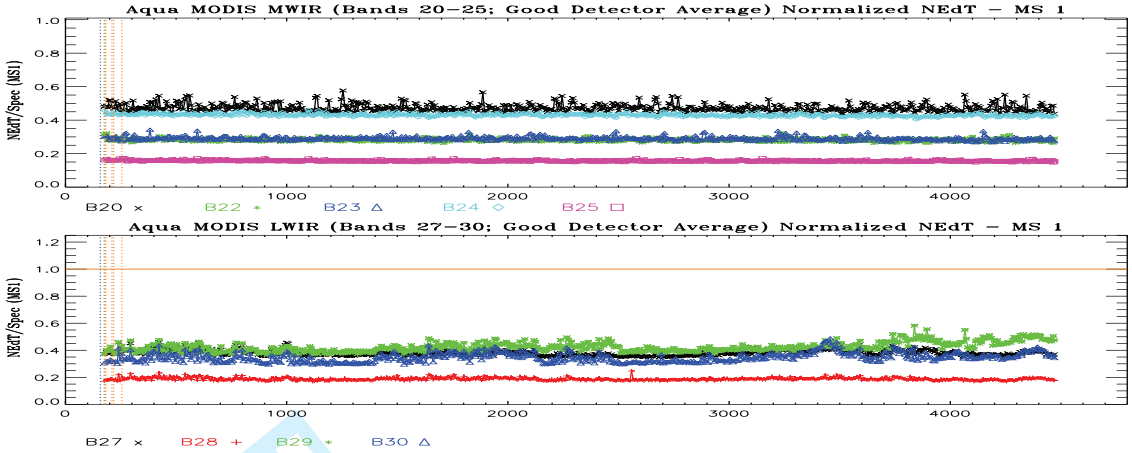

Fig. 9. Long-term NEdT trending for PV LWIR bands of A-MODIS

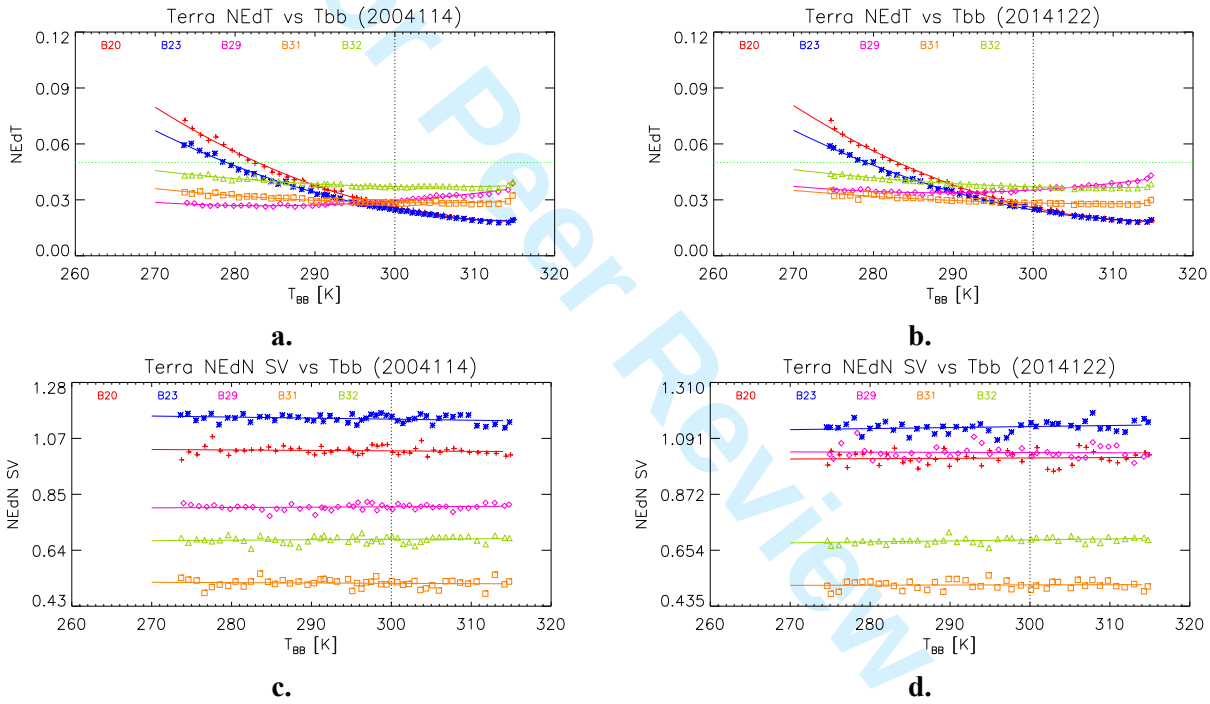

Fig. 10. Noise Characterization during BB WUCD operation for representative bands of T-MODIS a., c., 2004, b., d., 2014

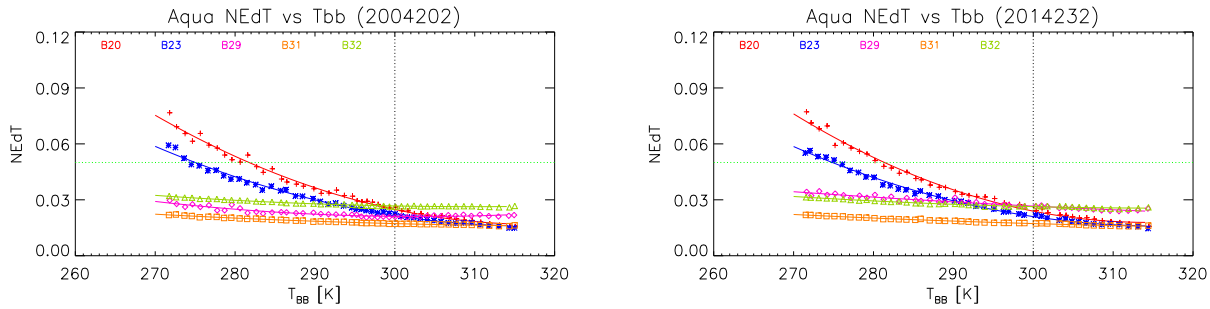

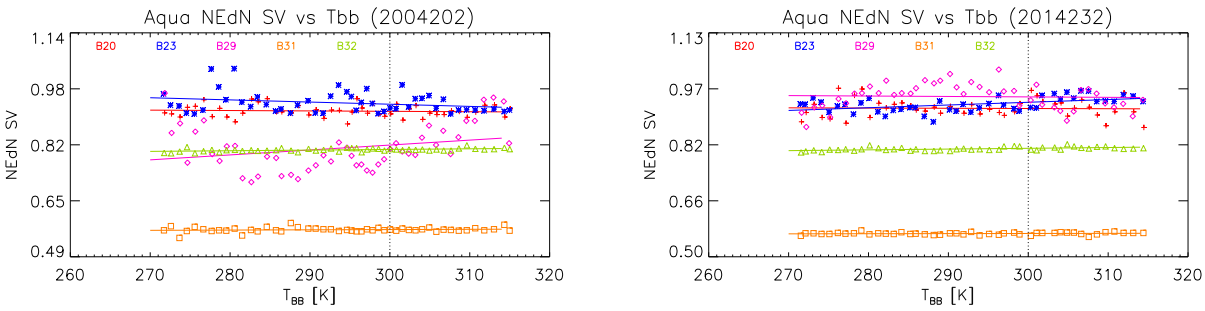

c. **d.**

Fig. 11. Noise Characterization during BB WUCD operation for representative bands of A-MODIS a., c., 2004, b., d., 2014

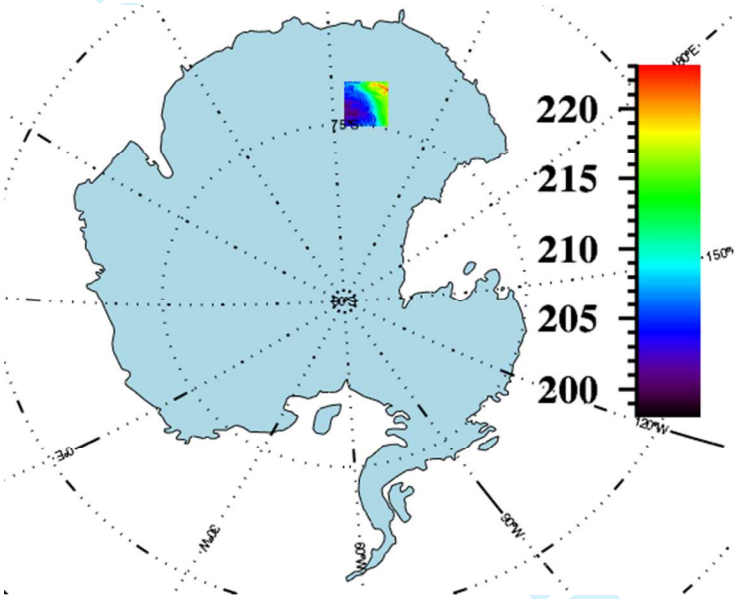

Fig. 12. Example of Antarctic EV location comprising of nadir viewing Dome C site (400 km x 400 km image map of T-MODIS band 31)

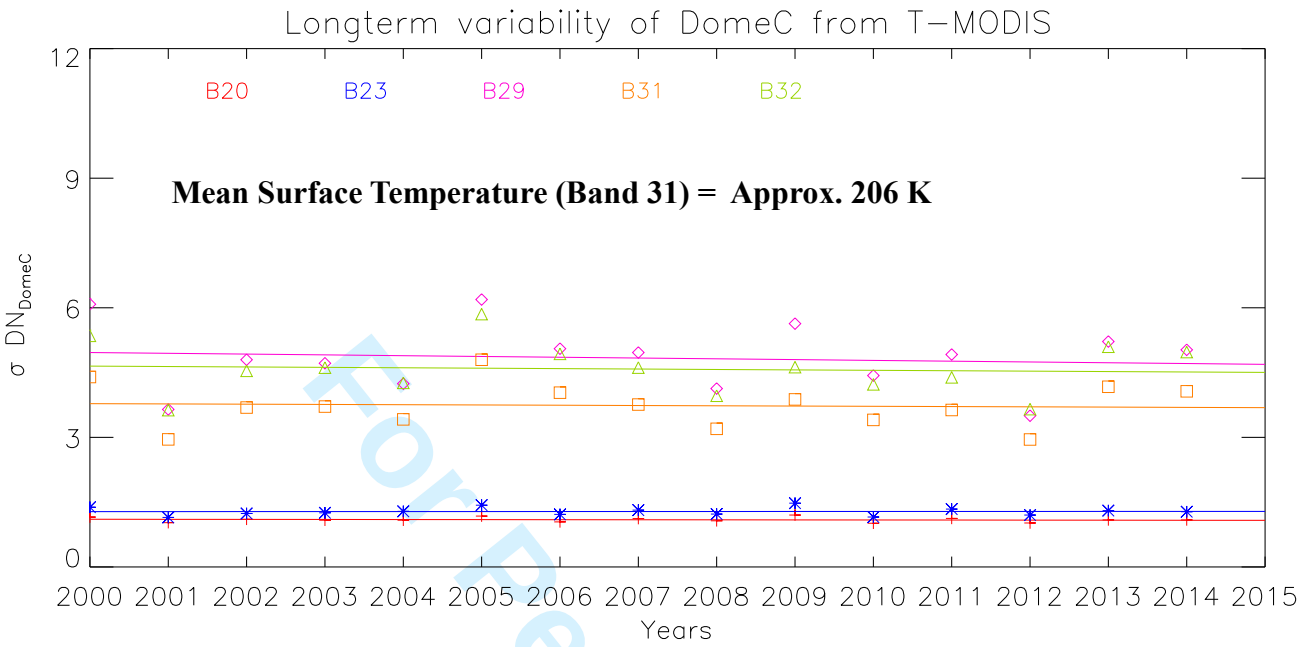

Fig. 13. Standard deviation characterization of Dome C EV site for representative bands of T-MODIS

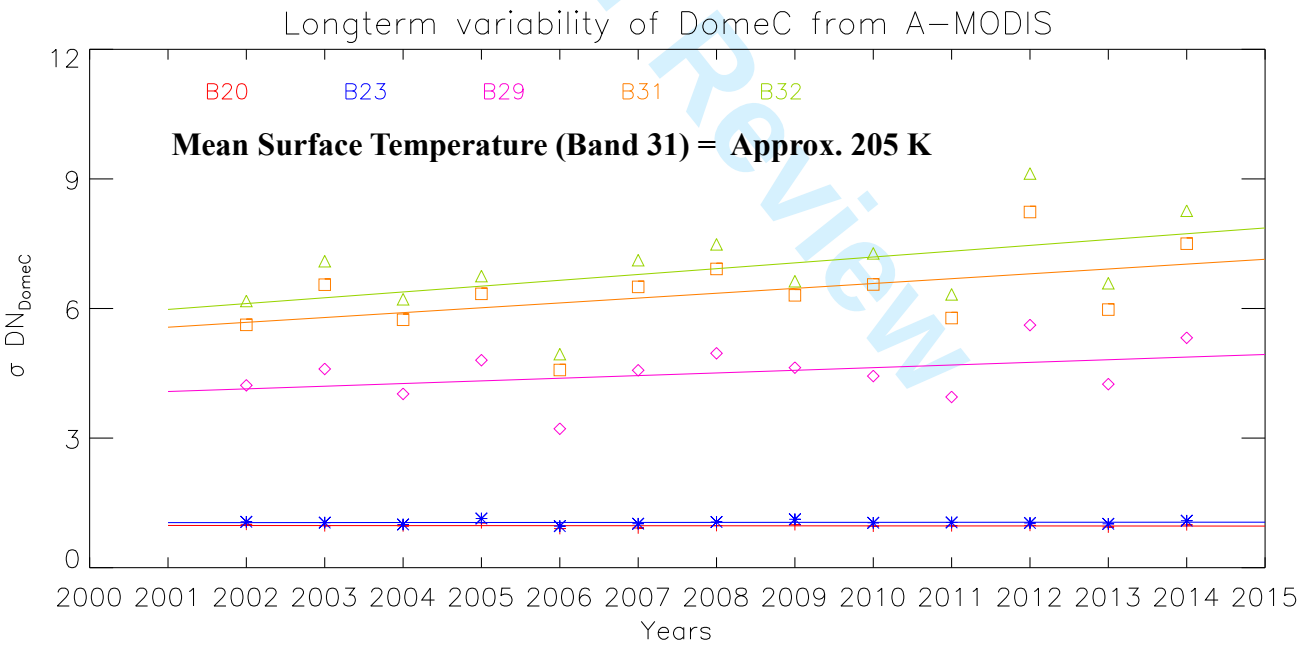

Fig. 14. Standard deviation characterization of Dome C EV site for representative bands of A-MODIS